Multitechnology (I-UWB and OFDM) Coexistent Communications on the Power Delivery Network

Andrea M. Tonello, *Senior Member, IEEE*, Fabio Versolatto, *Student Member, IEEE*, and Mauro Girotto, *Student Member, IEEE*

***Abstract*—To improve the performance and to support novel command and control applications in the smart-grid context, novel or alternative transmission schemes can be used in combination with existent power-line communication (PLC) solutions that are based on multicarrier or narrowband single carrier modulation schemes. In this respect, it is fundamental to ensure the coexistence between different systems yet respecting electromagnetic-compatibility (EMC) constraints. We consider the deployment of impulsive-ultrawideband (I-UWB) modulation for low-data-rate PLC. First, we study the design of the modulation parameters as a function of the application scenario. We consider the in-home, the outdoor low-voltage, and the outdoor medium-voltage scenario. Furthermore, we discuss EMC aspects and, according to the norms, we derive the limits for the power spectral density of the I-UWB signal. Then, we study the coexistence between existing orthogonal frequency-division multiplexing (OFDM) PLC solutions and I-UWB when they (partly) share the spectrum. We focus on the physical layer and we perform the analysis in terms of maximum achievable rate. The results show that I-UWB is suitable for low-data-rate applications and, further, it can coexist with existing OFDM PLC systems.**

***Index Terms*—Coexistence, multicarrier modulation, power-line communications (PLC), ultra-wideband (UWB) communications.**

I. Introduction

POWER-LINE communications (PLC) is an established solution to deliver information data by exploiting the existent power delivery infrastructure. Recently, PLC is gaining interest as a reliable communication solution for the smart grid (SG). The management of the SG is based on command and control services that require robust, low-data-rate communications. In this respect, PLC has been proven to be a valid candidate for the outdoor low-voltage (O-LV), and the medium-voltage (O-MV) scenario [1]. Furthermore, the SG concept is being applied to the in-home (IH) scenario, where home automation networks enable energy-management applications.

Several standards have been developed for IH and outdoor PLC. They provide specifications for broadband (BB) PLC and narrowband (NB) PLC. BB-PLC occupies the higher frequency range, and it ensures high-speed communications. Existing standards operate in the 2–30 MHz band, where the uppermost frequency is now limited by the electromagnetic-compatibility (EMC) norms on the conducted emissions. NB-PLC is intended for low-data-rate communications. In Europe, NB-PLC operates in the Cenelec bands defined by the standard EN 50065. These bands are located in the range of frequencies between 3 and 148.5 kHz. In the U.S. and Japan, the NB-PLC devices operate in the Federal Communicatons Commisssion (FCC) band 9–490 kHz and in the ARIB band 10–450 kHz, respectively.

Formerly, NB-PLC was based on single carrier modulation. For instance, spread-frequency-shift keying (S-FSK) [2] was adopted by the International Electrotechnical Commission (IEC) in standard IEC 61334. S-FSK has been largely deployed for low-date-rate services. More recently, multicarrier modulation schemes based on orthogonal frequency-division multiplexing (OFDM) or its variants, as pulse-shape OFDM, were considered for high-rate NB-PLC and BB-PLC.

Alternative modulation schemes are possible. In this respect, we study the possibility of using impulsive-ultrawideband (I-UWB) modulation [3] for command and control applications. The idea behind impulsive modulation is to map the information symbols into short duration pulses, namely, monocycles that are followed by a guard time during which the transmitter is silent. The guard time copes with the channel time dispersion, and, if it is sufficiently long, we do not experience intersymbol interference (ISI). According to the FCC, impulsive modulation can be classified as UWB if the fractional bandwidth, that is, the ratio between the signaling bandwidth and the central frequency is larger than 0.2. The transmitter is simple, and it consists of a pulser. The receiver is based on the matched-filter (MF) concept.

The first attempt toward the use of I-UWB in PLC was investigated in the European project Wirenet [4]. Practical receiver algorithms for in-home multiuser high-speed I-UWB communications in the IH scenario were studied in [5] and, more recently, the application of I-UWB for outdoor low-voltage PLC was analyzed in [6]. The use of WiMedia multiband OFDM over power lines was recently investigated in [7]. Herein, we focus on low-data-rate applications. In detail, the idea is to spread the low-data-rate information over a broad frequency range. The main advantages are as follows. First, I-UWB is robust against NB interference. Second, given a power constraint, I-UWB operates with a low level of power spectral density (PSD) that yields a negligible level of conducted emissions. Third, the complexity of the I-UWB system is at least at the transmitter, less than that of a conventional OFDM transmitter. Despite the advantages, the I-UWB signal may occupy the same spectrum of other PLC systems. Therefore, it is interesting to study whether

Manuscript received April 20, 2012; revised December 31, 2012 and April 12, 2013; accepted May 21, 2013. Date of current version September 19, 2013. Paper no. TPWRD-00411–2012.

The authors are with the Dipartimento di Ingegneria Elettrica, Gestionale e Meccanica, DIEGM, Università di Udine, Udine 33100, Italy (e-mail: tonello@uniud.it; fabio.versolatto@uniud.it; mauro.girotto@uniud.it).

Color versions of one or more of the figures in this paper are available online at http://ieeexplore.ieee.org.

Digital Object Identifier 10.1109/TPWRD.2013.2264881

coexistence is possible and to investigate the coexistence mechanisms. In this respect, a comparison in EMC terms between OFDM and I-UWB was presented in [8].

In this paper, we focus on the physical layer (PHY). First, we discuss the optimal design of the I-UWB parameters as a function of the application scenario. We consider the EMC aspects concerning PLC, and we derive the PSD transmission limits. Then, we study the achievable rate of both systems when they are deployed simultaneously in order to address the performance degradation due to the interference. The results are affected by service and traffic models. In order to address the lower-performance bound, we focus on the worst case scenario, namely, when the communications are uninterrupted and simultaneous. In this respect, we note that further coexistence mechanisms based on carrier-sense multiple-access (CSMA) protocols can be adopted at the MAC layer. In this respect, the norm EN 50065 forces the use of CSMA for communications in the CENELEC C band.

In the IH scenario, we study the coexistence between I-UWB and BB-OFDM. Indeed, in the outdoor scenario, we focus on the coexistence between I-UWB and NB-OFDM because NB-PLC is considered to be the most suitable technology for SG applications.

The remainder of this paper is organized as follows. In Section II, we describe the I-UWB system with a particular emphasis on the pulse-shape design. In Section III, we describe the OFDM scheme and we provide the parameter values that we use to simulate BB and NB OFDM PLC according to the standards. In Section IV, we review the EMC norms, from which we derive the PSD limits for both OFDM and I-UWB. In Section V, we deal with the coexistence at the PHY layer. Then, in Section VI, we describe the application scenarios, and we provide several numerical results. Finally, the conclusions follow.

II. Impulsive WideBand Modulation

I-UWB maps the information symbols into short duration pulses that are followed by a guard time. The transmitted signal is as follows:

$$s_u(t) = \sum_{k\in\mathbb{Z}} b_k g_{tx}(t - kT_{f,u}) \tag{1}$$

where b_k is the kth information symbol, $T_{f,u}$ is the duration of the I-UWB frame, and $g_{tx}(t)$ is the transmission pulse, namely, the monocycle. We shape the monocycle as one of the derivatives of the Gaussian pulse. Then, we transmit the signal in (1) over the PLC channel with impulse response $g_{ch}(t)$.

The receiver is based on the MF concept and it is optimal in the absence of ISI. Basically, we filter the received signal with an MF, namely, $g_{rx}(t)$, and we sample the output signal with period $T_{f,u}$ to obtain $\Lambda(kT_{f,u})$. When the modulation is binary, we decide for the received bit in the kth frame as $b_k = sign\{\Lambda(kT_{f,u})\}$.

The impulse response of the matched filter is a function of the channel and the noise. When the noise is not white, as in PLC, the impulse response of the MF receiver is equal to $g_{rx}(t) = g_{\text{eq}}^{-}(t) * R_d^{-1}(t)$, where $g_{\text{eq}}^{-}(t) = g_{tx} * g_{ch}(-t)$, and $R_d^{-1}(t)$ is the convolutional inverse of the noise correlation $R_d(t)$ (i.e., $R_d^{-1} * R_d(t) = \delta(t)$). We refer to this receiver as a noise-matched filter (N-MF) [9].

Practical receiver algorithms that are based on the MF concept were presented in [5] and [9], and recently their performances were compared in [10].

A. Gaussian Pulse-Shape Design

The idea of shaping the monocycle as one of the derivatives of the Gaussian pulse comes from the wireless scenario [11]. In PLC, the derivatives of the Gaussian pulse are suitable as well. In fact, they avoid transmitting in the lower frequency range, where we experience the highest levels of man-made noise. The Gaussian pulse reads as follows:

$$g_0(t) = \frac{K_0}{\sqrt{2}T_0} e^{-\frac{\pi}{2}\left(\frac{t}{T_0}\right)^2} \tag{2}$$

where T_0 and K_0 determine the transmission bandwidth and the energy of the transmitted pulse, respectively. In Section IV, we will determine the value of K_0 to be compliant with the EMC constraints on conducted emissions. The frequency response of the pth derivative of the Gaussian pulse reads

$$G_p(f) = \mathcal{F}\left[\frac{d^p}{dt^p} g(t)\right](f) = K_0 (i2\pi f)^p e^{-2\pi T_0^2 f^2} \tag{3}$$

where $\mathcal{F}[\cdot]$ denotes the Fourier transform operator. In particular, we note that (3) is maximum at the frequency

$$f_{\max,p} = \frac{\sqrt{p}}{2\sqrt{\pi}T_0}. \tag{4}$$

We consider the two frequencies for which (3) falls 10 dB below its maximum. We denote them as f_l and $f_h > f_l$, and we note that $f_l = 0$ in the case of the Gaussian pulse. Then, we define the transmission bandwidth as $B = f_h - f_l$. The transmission bandwidth is a function of T_0. For the Gaussian pulse, we obtain

$$T_0 = \sqrt{\frac{\ln 10}{4\pi B^2}}. \tag{5}$$

In the case of the derivatives of the Gaussian pulse, the former relation is more convoluted, and we obtain the value of T_0 that leads to a transmission bandwidth B as follows. We vary T_0 and we find f_l and f_h that solve

$$\left(2\sqrt{\frac{\pi}{p}} T_0 f\right)^{2p} e^{-4\pi T_0^2 f^2 + p} = 10^{-1}. \tag{6}$$

Then, we choose the value of T_0 for which $f_h - f_l$ is equal to the desired bandwidth B. Numerically, we have found that T_0 is approximately independent from the derivative order.

III. Multicarrier Modulation

Multicarrier modulation, in the form of OFDM, deploys M sub-channels at the transmitter side. The transmission bandwidth is $B_o = 1/T_s$ and the complex transmitted signal is

$$s_o(t) = K_0 \sum_{n\in\mathbb{K}_{ON}} \sum_{k\in\mathbb{Z}} b^{(n)}(kT_{f,o}) g(t - kT_{f,o}) W_{MT_s}^{-nt} \tag{7}$$

where $b^{(n)}(kT_{f,o})$ is the kth information symbol that is transmitted on the nth subchannel, $T_{f,o} = MT_s$ is the symbol period, $\mathbb{K}_{ON}$ denotes the set of used subchannels, that is, $\mathbb{K}_{ON} \subseteq \{0, \ldots, M-1\}$, $W_{MT_s}^{-nt} = \exp\{i2\pi nt/(MT_s)\}$, $g(t) = 1$ for $|t| < 1/(2T_{f,o})$, and 0 otherwise, and K_0 is the constant that defines the power of the transmitted signal.

The transmitter can be digitally implemented in the discrete-time domain with an M-points inverse discrete Fourier transform (IDFT). We let the sampling period be T_s. The output of the IDFT is extended with a cyclic prefix (CP) of μ samples, that is, $N = \mu + M$, $N \geq M$. At the receiver, we first acquire symbol synchronization. Then, we discard the μ samples that belong to the CP, and we process the remaining M samples with an M-points discrete Fourier transform (DFT). Finally, we perform zero-forcing single-tap subchannel equalization.

We do not experience intersymbol interference (ISI) if the CP length is greater than the maximum time dispersion that is introduced by the PLC channel.

A. Broadband OFDM

We adopt the parameters that were specified by the HomePlug AV standard [12]. Basically, we deploy 1536 sub-channels in the 2–28 MHz frequency range. We let the length of the frame duration and the cyclic prefix be equal to 40.96 μs, and 5.56 μs, respectively. Furthermore, we adopt the notching mask of HomePlug AV, as specified in Section IV.

B. Narrowband OFDM

Two OFDM relevant standards for NB-PLC are PRIME [13] and G3-PLC [14]. They are intended for outdoor PLC, and they ensure communications of up to 128 and 34 kbps, respectively, by signaling in the Cenelec bands. A comparison between G3 and PRIME was reported in [15], and was shown that they perform similarly. In the following, we adopt the modulation parameters of G3-PLC. We let the sampling frequency of the baseband system and the number of subchannels be 200 kHz and 128, respectively. According to the standard, we switch on only 36 sub-channels in the 35.9–90.6 kHz, i.e., in the effective transmission bandwidth. We set the symbol period and the CP duration equal to 640 μs and 75 μs, respectively for both O-LV and O-MV scenarios.

IV. EMC and PSD-Related Aspects

The transmitted PLC signal propagates according to two different modes, namely, the differential (symmetric) and the common (asymmetric) mode. Symmetric currents flow with the same intensity, but with opposite direction, through the power line wires, namely, the phase and the neutral. Indeed, the asymmetric currents flow with the same intensity and direction on both the phase and the neutral. For the common-mode (CM) currents, the conductors can be conceived as being a single wire, and the electrical circuit to be closed through a different path, for example, the physical earth. When the propagation mode is differential, the radiated field intensity is negligible because the currents flow in opposite directions. On the contrary, weak CM currents turn into strong radiated fields. In this respect, emission limits were defined by regulation bodies. The International Electrotechnical Commission (IEC) defines different limits for the frequency ranges up to, and above 30 MHz. In the lower frequency range, the focus is on conducted emissions, and the regulations constrain the maximum amplitude of the asymmetric signal that can be injected into the power delivery network. Above 30 MHz, the limits concern the radiated emissions. The conducted and radiated emission limits are described in the CISPR 22 norm. The measurement procedures are defined in the norm CISPR 16. Current BB-PLC standards fulfill limitations on conducted emissions because they operate in the 2–30 MHz frequency range. Limitations on the mains port, which coincides with the telecommunication port, define the PLC transmission levels [16]. According to CISPR 22, the average value of the CM component amplitude must be lower than $V_{lim} = 46$ dBμV and $V_{lim} = 50$ dBμV in the 0.5–5 MHz and the 5–30 MHz frequency range, respectively.

PLC employs differential mode signals. However, the asymmetries of the PLC network lead to the partial conversion of the differential mode currents into CM components. The relation between the amplitude of the symmetric signal transmitted from a port of the PLC network and the amplitude of the asymmetric component received at any other port of the network is referred to as transverse conversion transfer loss (TCTL) [16]. The TCTL is expressed in dB and it is a positive quantity. Experimental measurement campaigns in the IH scenario have shown that in 80% of the cases the amplitude of the common mode signal that is measured at any port of the network is at least 45 dB lower than the amplitude of the differential mode signal injected into the network, that is, $\mathrm{TCTL} \geq 45$ dB. In [16], the maximum PSD of the PLC signal that can be injected for transmission is computed as follows:

$$P_{lim} = V_{lim} + \mathrm{TCTL} - 10\log_{10}(B_{if}) - \nu \quad \left[\frac{\mathrm{dBm}}{\mathrm{Hz}}\right] \quad (8)$$

where $\mathrm{TCTL} = 45$ dB, B_{if} is the intermediate frequency bandwidth of the spectrum analyzer that is used to carry out the EMC measurements, and ν is the coefficient that allows for the conversion from dBμV to dBm, i.e., $\nu = 110$ dBm/μV. CISPR 16-1 sets $B_{if} = 9$ kHz. Now, if we assume a 100 Ω reference resistance, that is, a typical value for the power line characteristic impedance, and we let $V_{lim} = 50$ dBμV, we obtain $P_{lim} = -54.5$ dBm/Hz. The approximated value -50 dBm/Hz is often used by broadband PLC modems. Furthermore, the HomePlug consortium introduced the notching mask concept [12], [17]. In Fig. 1(a), we show the HomePlug notching mask. Basically, the notching mask reduces the transmitted PSD below -80 dBm/Hz at the frequencies where radio services are supposed to transmit. Multi-carrier modulation schemes, as OFDM, satisfy the notching mask by switching off certain subchannels. In Fig. 1, we also show the measured PSD of commercial modems during typical operating conditions. For a HomePlug-compliant device [BB-OFDM, Fig. 1(a)], the measured PSD satisfies the notching mask, and it is below -80 dBm/Hz in correspondence of the notched bands. For G3-PLC compliant devices [14] [NB-OFDM, Fig. 1(b)], the transmitted PSD level is approximately equal to -30 dBm/Hz, according to the European regulation limits that are less severe in the lower frequency range [18].

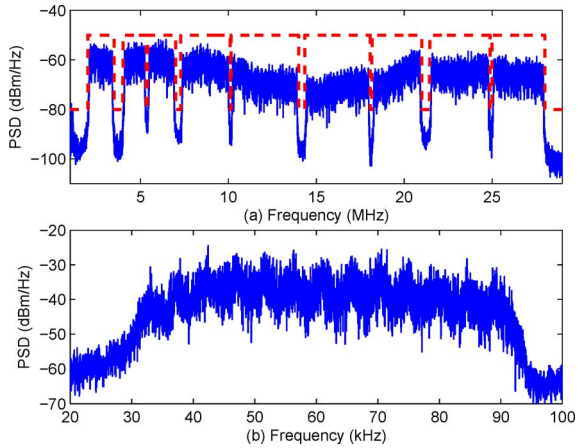

Fig. 1. Measurement results on the transmitted PSD level. On top, the transmitted PSD of a HomePlug-compliant device. The Homeplug notching mask is also shown. On the bottom, the transmitted PSD of a G3-PLC-compliant device that operates in the 32–95 kHz band (Cenelec A).

In the following, we assume the PSD of broad band OFDM to be equal to the HomePlug notching mask, and the PSD of narrow band OFDM to be limited to -30 dBm/Hz. Notching is rather complex for I-UWB. Therefore, we limit the PSD of the I-UWB signal to -80 dBm/Hz. In this respect, we note that preliminary studies on the radiated emissions of PLC systems that operate beyond 30 MHz pointed out that the PSD level of -80 dBm/Hz enables satisfying the radiated emission limits [19]. Furthermore, it enables satisfying the most severe conducted emission limits specified for the class B devices (IH use) in the entire frequency range below 30 MHz [20].

Now to proceed, we assume the information symbols to be independent and identical distributed with power M_b, and we use a unified notation for both OFDM and UWB. From (7) and (1), we can compute the average PSD of the transmitted signal as follows:

$$P_m(f) = 10\log_{10}\left(\frac{M_b}{T_{f,m}R_0}\sum_{n\in\mathbb{K}_m}\left|G_m^{(n)}(f)\right|^2\right),\ \left[\frac{\text{dB}}{\text{Hz}}\right] \tag{9}$$

where the pedix $\{\cdot\}_m$ denotes the modulation scheme, namely, $m \in \{o,\ u\}$, and $G_m^{(n)}(f)$, $T_{f,m}$, $\mathbb{K}_m$, and R_0 are the frequency response of the prototype pulse of the nth subchannel, the frame period, the number of active carriers, and the reference resistance, respectively. Furthermore, M_b is the statistical power of the information symbol b. The statistical power of the random process $x(t)$ reads $M_x = E[|x(t)|^2]$, where $E[\cdot]$ denotes the expectation. In the following text, we assume $R_0 = 100\ \Omega$, and $M_b = 1$.

In OFDM, $\mathbb{K}_o$ is the set of active sub-channels. According to the notation of Section III, $G_o^{(n)}(f)$, is the frequency response of $g^{(n)}(t)$. In I-UWB, $\mathbb{K}_u = 1$ because the transmission is single-carrier. It follows that $G_u^{(1)}(f)$ is the frequency response of the I-UWB monocycle. Furthermore, while OFDM transmits with a PSD level that is strictly equal to the limit in the whole transmission band, I-UWB meets the limit of -80 dBm/Hz only at $f = f_{\max}$ and it is always smaller elsewhere. This is beneficial in terms of both interference and emissions [8]. In the following, we refer to $P_{\max}$ as the maximum PSD value of the I-UWB transmission, that is, $P_{\max} = P_u(f_{\max})$.

From the PSD limit, we can derive the value of the scaling factor K_0 in (3). Exploiting (3), (4), and (9), we obtain

$$K_0 = \left(\frac{T_0}{\sqrt{p\pi}}\right)^p \sqrt{T_{f,u}10^{\frac{P_{\max}}{10}}R_0 e^p} \tag{10}$$

where p is the order of the derivative of the Gaussian pulse. The former relation allows scaling the I-UWB pulse as a function of the frame duration, and the PSD limit.

V. Coexistence at the PHY Layer

The PLC physical layer is a shared medium. Thus, the coexistence concept is important. In the literature, only few works deal with this subject, and they all focus on BB-PLC [21]–[25].

In this section, we address the coexistence between OFDM and I-UWB, when they (partially) share the spectrum. We investigate the performance of one system when the other is also operating. We model the latter as noise, and we follow a conservative approach, that is, we assume the communications to be uninterrupted and simultaneous. We describe the impact of one system to the other in terms of achievable rate. We assume the transmitted signals to be zero-mean, uncorrelated, and normally distributed, and the noise to be Gaussian and colored. We consider different application scenarios, and for each scenario, we define two configurations, namely, the worst and the best case. In the best case, the system of interest transmits over the best channel and the interfering system transmits over the worst channel. We define the best and the worst channel according to their Shannon capacity, as described in Section VI-A. Conversely, in the worst case, the signal of interest and the interference are transmitted through the worst and the best channel, respectively.

A. Effect of I-UWB on OFDM

We herein consider the impact of I-UWB modulation on the OFDM system. At the receiver, the output of the DFT is

$$z^{(n)}(kT_{f,o}) = b^{(n)}(kT_{f,o})G_{ch}^{(n)} + D^{(n)}(kT_{f,o}) \tag{11}$$

where n, $G_{ch}^{(n)}$, and $D^{(n)}(kT_{f,o})$ are the subchannel index, the M-point DFT of the channel impulse response between the OFDM transmitter and the OFDM receiver at the nth subchannel, and the M-point DFT of the disturbance of the kth frame at the nth subchannel, respectively. Assuming the absence of ISI and ICI, the disturbance reads

$$D^{(n)}(kT_{f,o}) = W^{(n)}(kT_{f,o}) + I_u^{(n)}(kT_{f,o}) \tag{12}$$

where $W^{(n)}(kT_{f,o})$ is the M-points DFT of the background noise samples of the kth frame, and $I_u^{(n)}(kT_{f,o})$ is the interference caused by I-UWB. For simplicity, we assume the frame duration of I-UWB to be an integer submultiple of the OFDM frame. Thus, each OFDM frame contains an integer number of I-UWB pulses.

Under this assumption, the interference due to I-UWB on the OFDM received signal is

$$I_u^{(n)}(kT_{f,o}) = \sum_{r=0}^{M/Q-1} b_r e^{-2\pi f_n rQ} G_{\text{eq}}^{(n)} \tag{13}$$

where n is the subchannel index, Q is the number of I-UWB frames per OFDM frame, b_r is the rth I-UWB symbol that is transmitted in the kth OFDM frame, $G_{eq}^{(n)}$, $n = 0, \ldots, M-1$ is the M-points DFT of $g_{eq} * g_{ch}(lT_s)$, where $g_{ch}(t)$ is the channel impulse response between the I-UWB transmitter and the OFDM receiver.

According to the previous assumptions on the statistics of the transmitted signal and the noise, we can express the maximum achievable rate of the OFDM system as

$$C_o = \frac{1}{T_{f,o}} \sum_{n=0}^{M-1} \log_2 \left(1 + \frac{M_b^{(n)} \left| G_{ch}^{(n)} \right|^2}{M_{I,u}^{(n)} + M_W^{(n)}} \right) \quad [\text{bit/s}] \tag{14}$$

where $M_b^{(n)}$, $M_W^{(n)}$, and $M_{I,u}^{(n)}$ denote the information symbol, the noise, and the I-UWB interference statistical power for subchannel n, respectively.

B. Effect of OFDM on I-UWB

We now analyze the interference generated by the multicarrier modulation system on the I-UWB system. The output of the MF can be written as

$$u(kT_{f,u}) = b_k g_{\text{eq}} * g_{rx}(0) + I_o(kT_{f,u}) + \eta(kT_{f,u}) \tag{15}$$

where $I_o(kT_{f,u})$ is the interference that is caused by OFDM and $\eta(kT_{f,u})$ is the background noise. The OFDM interference can be written as

$$I_o(kT_{f,u}) = s_o * g_{ch} * g_{rx}(kT_{f,u}) \tag{16}$$

where $s_o(t)$ is the OFDM transmitted signal, and $g_{ch}(t)$ is the channel impulse response between the OFDM transmitter and the I-UWB receiver. We define the maximum achievable rate of the I-UWB system as

$$C_u = \frac{1}{T_{f,u}} \log_2 \left(1 + \frac{M_b |g_{eq} * g_{rx}(0)|^2}{M_{I,o} + M_\eta} \right), \quad [\text{bit/s}] \tag{17}$$

where M_b, $M_{I,o}$, and M_η are the statistical power of the I-UWB information symbol, the OFDM interference, and the background noise after the MF, respectively.

VI. Numerical Results

This section is organized as follows. First, we present the PLC application scenarios. Then, we design the I-UWB parameters for each scenario. Finally, we study the degradation of the achievable rate due to the simultaneous transmission of both systems. In our simulations, we use the N-MF receiver for I-UWB, and we assume that both systems transmit simultaneously and continuously. For OFDM, we distinguish between the IH scenario and the outdoor scenarios. In the IH scenario, we consider BB-OFDM. In the outdoor scenarios, we focus on NB-OFDM. For I-UWB, we design the parameters according to the method described in Section VI-B. Finally, we show the minimum, the mean, and the maximum achievable rate in the presence or the absence of interference.

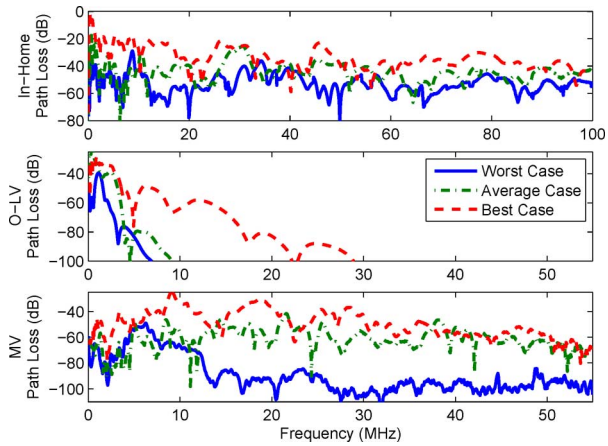

Fig. 2. Representative channels for the best, the average, and the worst case scenario. From top to bottom, the in-home, outdoor low-voltage, and medium-voltage scenarios are shown.

A. PLC Application Scenarios

1) In-home: We performed a broad band measurement campaign in Italy. The channels were measured up to 100 MHz in different premises that are representative of small flats and detached houses of 50–100 m^2. We measured the channels between all possible combinations of outlets. We collected a total amount of 331 direct and reverse channels.

2) Outdoor LV: For the outdoor LV scenario, we exploit the models presented in the literature and obtained from measurements. In [26], the analytic expression of eight representative channels is given. We extend the validity of the analytic representation up to 55 MHz. However, we note that the attenuation strongly increases with the frequency and even in the best case, we already experience more than 100 dB of attenuation at 30 MHz.

3) Outdoor MV: We consider the 20-kV medium-voltage (MV) network that we described in [27]. It is a real-life MV network that feeds a large number of industrial users concentrated in a small area. We acquired a total amount of 42 links. Among these, eight lack of electrical continuity because the receiver was isolated from the rest of the network by an open switch. Measurement results have validity up to 55 MHz.

In all three scenarios, we have selected three representative channels, that is, one for the worst, one for the average, and one for the best case. In Fig. 2, we show the path loss of the channels. For each scenario, we have computed the Shannon capacity of the channels and the cumulative distribution function (CDF) of the capacity. Then, we have selected the representatives as the ones whose capacity corresponds to the 20th, 50th, and 80th percentile of the CDF.

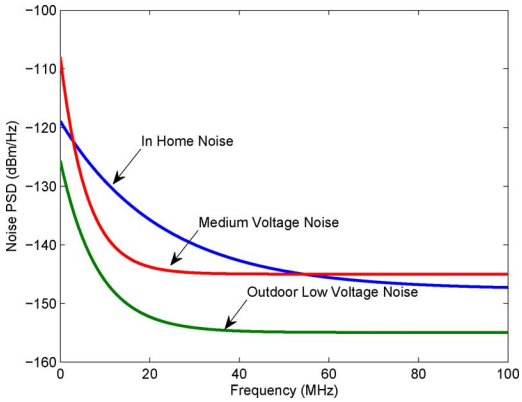

Fig. 3. Broadband noise power spectral density (PSD) for the in-home, outdoor low-voltage, and medium-voltage PLC scenarios.

TABLE I
PARAMETERS OF THE I-UWB SYSTEM FOR INHOME AND OUTDOOR SCENARIOS DESIGNED AS EXPLAINED IN SECTION VI-B

Scenario	Pulse Shape	B [MHz]	$T_f u$ [μs]	Rate [MPulses/s]
IH	4th derivative	25	0.4096	2.44
O-LV	Gaussian	10	1.25	0.80
O-MV	2nd derivative	20	0.64	1.56

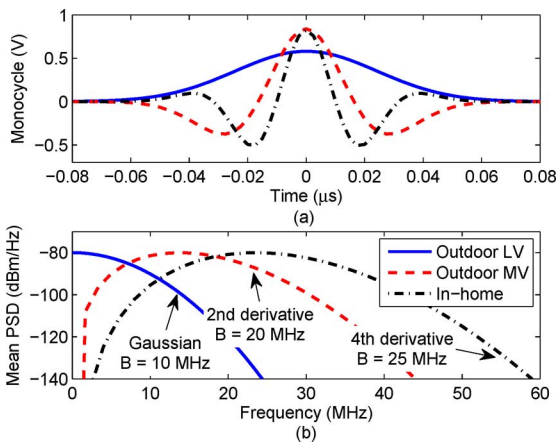

Fig. 4. On the top, the optimal transmission pulses for each scenario. On the bottom, the mean PSD of the transmitted signal.

We model the background noise as additive colored Gaussian noise. In Fig. 3, we show the noise models of the three scenarios that we consider. The models have been presented for the broadband case in [26], and we extend their validity to low frequencies. The PSD profiles follow an exponentially decreasing rule.

B. Design Parameters

The optimal design of the I-UWB parameters is a complex multivariate optimization problem with four variables (i.e., the pulse shape, the transmission bandwidth, the frame period, and the PSD level). We aim to identify the pulse that yields to a bit-error rate (BER) below a target value with the lowest transmission bandwidth. The details of the procedure are reported in Appendix A.

We have performed the optimization for all three application scenarios, and we report the results in Table I. In Fig. 4, we show the optimal monocyles for each scenario and the mean PSD of the transmitted signal, assuming a maximum level of -80 dBm/Hz. In the IH scenario, we propose the use of the 4th derivative of the Gaussian pulse whose spectral contribution in the CENELEC A band is well below -170 dBm/Hz, namely, it can be neglected and it fulfills the European norms EN 50065-1.

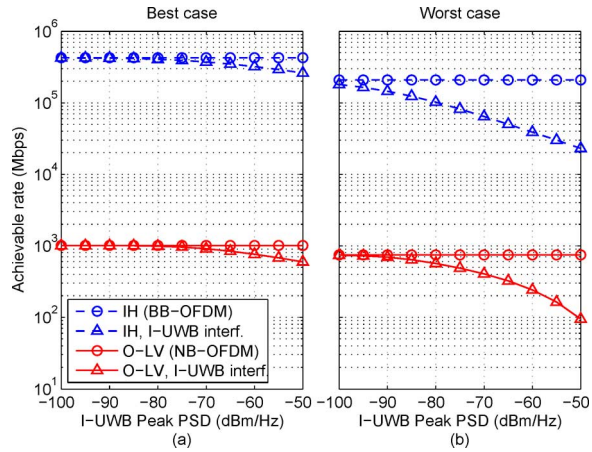

Fig. 5. Achievable rate for OFDM in the presence of I-UWB as a function of the I-UWB monocycle peak PSD.

C. Coexistence

In this section, we study the decay of performance when I-UWB and OFDM systems transmit simultaneously sharing the spectrum. First, we focus on OFDM. In Fig. 5, we show the achievable rate of the OFDM system when the I-UWB transmission is, or is not, interfering. On the x axis, we report the maximum PSD level of the I-UWB transmission when it is present. We limit the study to the IH and O-LV scenarios because in the O-MV scenario, the systems do not interfere since they use disjoint spectra, and we provide the results for the best and the worst case, as defined in Section V. I-UWB uses the parameters of Section VI-B.

Let us focus on a I-UWB interferer at -80 dBm/Hz. In the best case, OFDM does not experience a performance decay. In the worst case, the performance decay due to I-UWB is still acceptable. For instance, in the IH scenario where the impact of I-UWB is more pronounced, the maximum achievable rate of the OFDM system is above 100 Mb/s and it is sufficient for high-speed multimedia communications. For the O-LV scenario, the performance decay is even less pronounced.

Now, we focus on the impact of OFDM on I-UWB. Again, we do not consider the O-MV scenario because the systems do not share the spectrum. In Fig. 6, we show the results. For the O-LV scenario, there is no significant impact on the I-UWB performance. For the IH scenario and the best case, the impact of OFDM is still negligible. Indeed, in the worst case, OFDM impacts more severely the achievable rate of I-UWB thought the I-UWB data rate is always acceptable for command and control applications.

It should be noted that the presence of interference may reduce the signal-to-noise ratio (SNR) margin and, thus, reduce coverage. In the considered scenarios, when I-UWB transmits

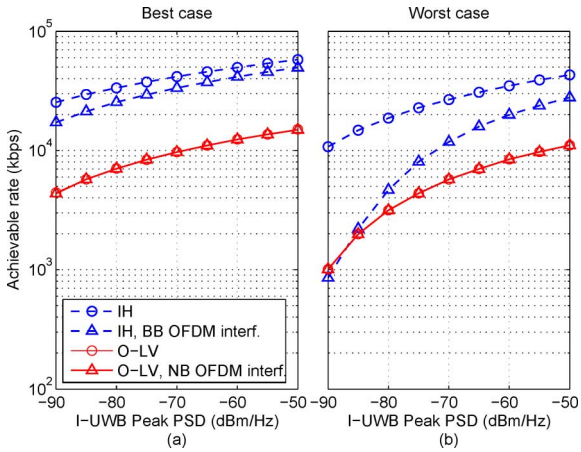

Fig. 6. Achievable rate for I-UWB in the presence of an OFDM interferer as a function of monocycle peak PSD.

TABLE II
ACHIEVABLE RATE FOR ALL SCENARIOS

		OFDM		I-UWB	
		No Interf.	Interf.	No interf.	Interf.
IH	min [Mbps]	209	102	18.7	4.7
	mean [Mbps]	288	226	28.9	13.2
	max [Mbps]	426	406	33.5	25.3
O-LV	min [Mbps]	0.75	0.57	3.16	3.12
	mean [Mbps]	1.11	0.83	5.51	5.47
	max [Mbps]	1.01	0.99	7.06	6.89
O-MV	min [Mbps]	0.19	-	1.6	-
	mean [Mbps]	0.27	-	11	-
	max [Mbps]	0.23	-	19.2	-

at −80 dBm/Hz, OFDM is not significantly affected, so that the coverage offered by OFDM does not change.

D. Achievable Rate for All Scenarios

Now, we analyze the mean, the minimum, and the maximum achievable rate of both systems when they operate in standalone mode or they transmit simultaneously. For the minimum achievable rate, we refer to the worst case, namely, the useful signal is filtered by the worst channel, and the interferer is filtered by the best channel. For the maximum achievable rate, we refer to the best case. For the mean achievable rate, we assume both signals to be filtered by the average channel. In Table II, we show the results. In the O-MV case, we do not report the values in the presence of interference because the systems do not share the spectrum. We consider BB-OFDM for the IH scenario, and NB-OFDM for the O-LV and O-MV scenario. For BB-OFDM, the PSD level is set at −80 dBm/Hz in the notched frequency bands and −50 dBm/Hz otherwise. For NB-OFDM, the PSD level is set at −30 dBm/Hz. For I-UWB, the PSD peak is set to −80 dBm/Hz.

In this respect, we note that the PSD limits that we consider, and that are adopted by the commercial systems, turn into a transmitted power of 18, 24, and −10 dBm, for NB-OFDM, BB-OFDM, and I-UWB, respectively. Thus, I-UWB transmits at a significantly lower power level than OFDM. In the IH scenario, I-UWB achieves a lower rate than BB-OFDM, but the two systems are designed for different purposes, that is, command and control applications and high-data-rate transmissions, respectively. In the outdoor scenarios, I-UWB exhibits higher rates than NB-OFDM. Therefore, it can be considered as a valuable alternative. Finally, the average rate is not largely affected by the simultaneous operation of the two systems.

VII. CONCLUSION

We have addressed the problem of coexistence between different modulation schemes for PLC, namely, OFDM and impulsive ultrawideband modulation. We have considered three application scenarios, that is, in-home, outdoor low voltage and outdoor medium voltage, and two OFDM schemes, that is, narrowband and broadband. First, we have described the EMC aspects and we have derived the limits of the PSD of the transmitted signal from EMC norms.

Then, we have addressed the design of the I-UWB parameters in all three application scenarios. The I-UWB monocycle belongs to the family of Gaussian derivative pulses and its band depends on the considered scenario.

Finally, we have studied the coexistence between OFDM and I-UWB in terms of maximum achievable rate for the same channel set, when the two systems operate simultaneously. We have found that by transmitting I-UWB signals with a maximum PSD of −80 dBm/Hz (which is significantly lower than the level deployed by existing PLC systems), we obtain reliable performance and sufficient coexistence with OFDM. In particular, in the IH scenario, BB-OFDM communications are still possible in the presence of I-UWB, while I-UWB can be used for medium-speed communications, for example, for command and control applications. In the O-LV scenario, NB-OFDM communications have a negligible impact on I-UWB, and, further, in the O-MV scenario, the systems do not share the spectrum because NB-OFDM transmits at lower frequencies. Therefore, in this case, the coexistence is ensured.

We note that coexistence mechanisms at the physical and MAC layer can be implemented to improve the performance as, for instance, the use of CSMA or interference cancellation method with appropriate signal-processing algorithms. The MAC layer can also handle coexistence and interconnectivity between I-UWB devices operating in different sections of the network.

As a final remark, we have not considered the coexistence between I-UWB and narrowband single carrier systems, for example, FSK modulation schemes. This is less problematic because of the intrinsic characteristics of the spread-spectrum I-UWB system that transmits with significantly lower PSD over a much wider spectrum. This generates low interference to narrowband single carrier systems. On the other side, the I-UWB system enjoys the high processing gain from spectrum expansion which renders the effect of a narrowband single carrier system negligible.

TABLE III
MAXIMUM VALUES OF THE PSD, IN dBm/Hz, FOR THE I-UWB SYSTEM USED TO DESIGN THE MONOCYCLE SHAPE AND THE BANDWIDTH

Scenario	Best channel	Average channel	Worst channel
In-home	-121	-112	-100
Outdoor LV	-116	-100	-78
Outdoor MV	-101	-100	-86

APPENDIX A
PULSE DESIGN PROCEDURE

As reported in Section VI-B, the optimal design of the I-UWB parameters is a complex multivariate optimization problem. To simplify the problem, we follow a two-step procedure. As a starting point, we consider only three possible pulse shapes, that is, the Gaussian pulse and its second and fourth derivatives. We let the bandwidth be lower than 30 MHz. We also set the value of $P_{\max}$ to obtain a target BER in the range of $10^{-1} - 10^{-5}$ in the three transmission scenarios with all of the considered pulses when the bandwidth is 30 MHz. This yields the values reported in Table III.

During the first step, we identify the best pulse and transmission bandwidth as the ones that ensure the target $\mathrm{BER} \leq 10^{-3}$ with the lowest transmitted power. In this respect, we remark that the lower the bandwidth, the lower the transmitted power, under the assumption of a given $P_{\max}$ value. Furthermore, in this step, we assume a sufficiently long frame duration so that we do not experience any ISI. We have found that $T_{f,u} = 5\ \mu$s is a suitable choice.

In the second step, we reduce the frame duration. A short frame would increase the peak data rate but, at the same time, it would introduce ISI as shown in (17). Thus, we choose the minimum frame length for which the effect of ISI is still negligible w.r.t. the background noise level so that the BER is not affected. We denote the optimal value of the frame period with $T_{f,\min}$. The value of $T_{f,\min}$ is 0.4, 1.2, and 0.6 μs for the IH, O-LV, and O-MV scenario, respectively. In the simulations, we assume a frame duration to be an integer submultiple of the OFDM frame duration, that is, the lowest submultiple greater than $T_{f,\min}$. In detail, we set the frame duration to 0.4096, 1.25, and 0.64 μs for the IH, O-LV, and O-MV scenario, respectively.

REFERENCES

[1] K. Razazian, M. Umari, A. Kamalizad, V. Loginov, and M. Navid, "G3-PLC specification for powerline communication: Overview, system simulation and field trial results," in *Proc. IEEE Int. Symp. Power Line Commun. Appl.*, Mar. 2010, pp. 313–318.

[2] T. Schaub, "Spread frequency shift keying," *IEEE Trans. Commun.*, vol. 42, no. 2/3/4, pp. 1056–1064, Feb./Mar./Apr. 1994.

[3] M. Z. Win and R. A. Scholtz, "Impulse radio: How it works," *IEEE Commun. Lett.*, vol. 2, no. 2, pp. 36–38, Feb. 1998.

[4] G. Mathisen and A. M. Tonello, "WIRENET: An experimental system for in-house powerline communication," in *Proc. IEEE Int. Symp. Power Line Commun. App.*, Mar. 2006, pp. 137–142.

[5] A. M. Tonello, "Wideband impulse modulation and receiver algorithms for multiuser power line communications," *EURASIP J. Advances Signal Process.*, pp. 1–14, 2007.

[6] A. L. S. Ferreira and M. V. Ribeiro, "A discussion about the suitability of uwb modulation for outdoor power line communication," in *Proc. IEEE Int. Symp. Power Line Commun. App.*, Apr. 2010, pp. 102–107.

[7] M. U. Rehman, S. Wang, Y. Liu, S. Chen, X. Chen, and C. G. Parini, "Achieving high data rate in multiband-OFDM UWB over power-line communication system," *IEEE Trans. Power Del.*, vol. 27, no. 3, pp. 1172–1177, Jul. 2012.

[8] G. Mekuria and H. Hirsch, "UWB pulse transmission over powerline channel," in *Proc. IEEE Int. Symp. Power Line Commun. App.*, Mar. 2007, pp. 308–313.

[9] A. M. Tonello, R. Rinaldo, and L. Scarel, "Detection algorithms for wide band impulse modulation based systems over power line channels," in *Proc. IEEE Int. Symp. Power Line Commun. App.*, Apr. 2004, pp. 367–372.

[10] F. Versolatto, A. M. Tonello, M. Girotto, and C. Tornelli, "Performance of practical receiver schemes for impulsive UWB modulation on a real MV power line network," in *Proc. IEEE Int. Conf. Ultra-Wideband*, Sep. 2011, pp. 610–614.

[11] R. A. Scholtz, R. J.-M. Cramer, and M. Z. Win, "Evaluation of the propagation characteristics of ultra-wideband communication channels," in *Proc. IEEE Antennas Propag. Soc. Int. Symp.*, Jun. 1998, vol. 2, pp. 626–630.

[12] Home Plug Alliance. 2005. [Online]. Available: www.homeplug.org

[13] "Narrowband orthogonal frequency division multiplexing power line communication transceivers for prime networks," Recommendation ITU-T G.9904 2012.

[14] "Narrowband orthogonal frequency division multiplexing power line communication transceivers for g3-plc networks," Recommendation ITU-T G.9903 2012.

[15] A. M. Tonello, S. D'Alessandro, F. Versolatto, and C. Tornelli, "Comparison of narrow-band OFDM PLC solutions and I-UWB modulation over distribution grids," in *Proc. IEEE Smart Grid Commun. Conf.*, Oct. 2011, pp. 149–154.

[16] H. C. Ferreira, L. Lampe, J. Newbury, and T. G. Swart, *Power Line Communications: Theory and Applications for Narrowband and Broadband Communications Over Power Lines*. Hoboken, NJ: Wiley, 2010.

[17] N. Weling, "Expedient permanent PSD reduction table as mitigation method to protect radio services," in *Proc. IEEE Int. Symp. Power Line Commun. App.*, Apr. 2011, pp. 305–310.

[18] *Signalling on low-voltage electrical installations in the frequency range 3 khz to 148,5 khz—Part 1: General requirements, frequency bands and electromagnetic disturbances*, EN 50065-1:2011, CENELEC, 2011.

[19] B. Praho, M. Tlich, P. Pagani, A. Zeddam, and F. Nouvel, "Cognitive detection method of radio frequencies on power line networks," in *Proc. IEEE Int. Symp. Power Line Commun. App.*, Apr. 2010, pp. 225–230.

[20] *Information Technology Equipment—Radio Disturbance Characteristics—Limits and Methods of Measurement*, CISPR22, ed.6.0, IEC, Sep. 2008.

[21] "Specification for a coexistence mechanism (access/in-home PLC)," OPERA, Deliverable WP2-D18, Dec. 2005.

[22] D. Arlandis, J. Barbero, A. Matas, S. Iranzo, J. Riveiro, and D. Ruiz, "Coexistence in PLC networks," in *Proc. IEEE Int. Symp. Power Line Commun. App.*, pp. 260–264.

[23] Technical Working Group of Consumer Electronics Powerline Communications Alliance (CEPCA), "Ensuring coexistence for high-speed powerline carrier applications," in *Proc. Int. Conf. Consum. Electron.*, Jan. 2006, pp. 155–156.

[24] V. Dominguez, "UPA proposal for the coexistence of PLC networks," in *Proc. Int. Conf. Consum. Electron.*, Jan. 2006, pp. 157–158.

[25] C. Muller, C. Lewandowski, C. Wietfeld, H. Kellerbauer, and H. Hirsch, "Coexistence analysis of access and indoor powerline communication systems for smart grid ICT networks," in *Proc. IEEE Int. Symp. Power Line Commun. App. (ISPLC)*, Mar. 2012, pp. 77–82.

[26] M. Babic *et al.*, "OPERA deliverable d5. Pathloss as a function of frequency, distance and network topology for various l V and MV European powerline networks," OPERA-IST Integrated Project No 507667, 2005.

[27] A. M. Tonello, F. Versolatto, and C. Tornelli, "Analysis of impulsive UWB modulation on a real MV test network," in *Proc. IEEE Int. Symp. Power Line Commun. App.*, Apr. 2011, pp. 18–23.

Andrea M. Tonello (M'00–SM'12) received the D.Eng. in electronics (Hons.) and the D.Res. in electronics and telecommunications degrees from the University of Padova, Padova, Italy, in 1996 and in 2003, respectively.

From 1997 to 2002, he was with Bell Labs-Lucent Technologies, Whippany, NJ, USA, first as a Member of the Technical Staff. Then, he was promoted to Technical Manager and appointed to Managing Director of the Bell Labs Italy division. In 2003, he joined the University of Udine, Udine, Italy, where he is an Aggregate Professor and the founder of the Wireless and Power Line Communications Lab. He is also the founder of the spin-off company WiTiKee. He is an Editor for the IEEE TRANSACTIONS ON COMMUNICATIONS.

Dr. Tonello received several awards, including the Distinguished Visiting Fellowship from the Royal Academy of Engineering, U.K., in 2010, and the IEEE VTS Distinguished Lecturer Award in 2011–2012. He is the Vice-Chair of the IEEE Communications Society Technical Committee on Power Line Communications.

Fabio Versolatto (S'10) received the D.Res. degree in telecommunication engineering and the Laurea Specialistica degrees in electrical engineering (Hons.) from the University of Udine, Udine, Italy, in 2009 and 2013, respectively.

His research interests are power-line communication channel modeling and digital communication algorithms.

Dr. Versolatto received the award for the best student paper presented at IEEE ISPLC 2010. He is a Research Fellow with the University of Udine.

Mauro Girotto (S'12) received the Laurea and Laurea Specialistica degrees in electrical engineering (Hons.) from the University of Udine, Udine, Italy, in 2008 and 2011, respectively, where he is currently pursuing the Ph.D. degree in telecommunication engineering.

His research interests are wideband modulation schemes for power-line communications.